JCI insight

Intercalated cell BKα subunit is required for flow-induced K^+ secretion

Rolando Carrisoza-Gaytan, … , Lisa M. Satlin, Thomas R. Kleyman

JCI Insight. 2020;5(8):e130553. https://doi.org/10.1172/jci.insight.130553.

Research Article | Cell biology | Nephrology

BK channels are expressed in intercalated cells (ICs) and principal cells (PCs) in the cortical collecting duct (CCD) of the mammalian kidney and have been proposed to be responsible for flow-induced K^+ secretion (FIKS) and K^+ adaptation. To examine the IC-specific role of BK channels, we generated a mouse with targeted disruption of the pore-forming BK α subunit (BKα) in ICs (IC-BKα–KO). Whole cell charybdotoxin–sensitive (ChTX-sensitive) K^+ currents were readily detected in control ICs but largely absent in ICs of IC-BKα–KO mice. When placed on a high K^+ (HK) diet for 13 days, blood [K^+] was significantly greater in IC-BKα–KO mice versus controls in males only, although urinary K^+ excretion rates following isotonic volume expansion were similar in males and females. FIKS was present in microperfused CCDs isolated from controls but was absent in IC-BKα–KO CCDs of both sexes. Also, flow-stimulated epithelial Na^+ channel–mediated (ENaC–mediated) Na^+ absorption was greater in CCDs from female IC-BKα–KO mice than in CCDs from males. Our results confirm a critical role of IC BK channels in FIKS. Sex contributes to the capacity for adaptation to a HK diet in IC-BKα–KO mice.

JCI insight

RESEARCH ARTICLE

Intercalated cell BKα subunit is required for flow-induced K+ secretion

Rolando Carrisoza-Gaytan,[1] Evan C. Ray,[2] Daniel Flores,[1] Allison L. Marciszyn,[2] Peng Wu,[3] Leah Liu,[4] Arohan R. Subramanya,[2,5] WenHui Wang,[3] Shaohu Sheng,[2] Lubika J. Nkashama,[2] Jingxin Chen,[2] Edwin K. Jackson,[6] Stephanie M. Mutchler,[2,6] Szilvia Heja,[1] Donald E. Kohan,[7] Lisa M. Satlin,[1] and Thomas R. Kleyman[2,5,6]

[1]Department of Pediatrics, Icahn School of Medicine at Mount Sinai, New York, New York, USA. [2]Department of Medicine, University of Pittsburgh, Pittsburgh, Pennsylvania, USA. [3]Department of Pharmacology, New York Medical College, Valhalla, New York, USA. [4]McGill University, Montreal, Quebec, Canada. [5]Department of Cell Biology and [6]Department of Pharmacology and Chemical Biology, University of Pittsburgh, Pittsburgh, Pennsylvania, USA. [7]Department of Medicine, University of Utah Health Sciences Center, Salt Lake City, Utah, USA.

BK channels are expressed in intercalated cells (ICs) and principal cells (PCs) in the cortical collecting duct (CCD) of the mammalian kidney and have been proposed to be responsible for flow-induced K+ secretion (FIKS) and K+ adaptation. To examine the IC-specific role of BK channels, we generated a mouse with targeted disruption of the pore-forming BK α subunit (BKα) in ICs (IC-BKα–KO). Whole cell charybdotoxin–sensitive (ChTX-sensitive) K+ currents were readily detected in control ICs but largely absent in ICs of IC-BKα–KO mice. When placed on a high K+ (HK) diet for 13 days, blood [K+] was significantly greater in IC-BKα–KO mice versus controls in males only, although urinary K+ excretion rates following isotonic volume expansion were similar in males and females. FIKS was present in microperfused CCDs isolated from controls but was absent in IC-BKα–KO CCDs of both sexes. Also, flow-stimulated epithelial Na+ channel–mediated (ENaC-mediated) Na+ absorption was greater in CCDs from female IC-BKα–KO mice than in CCDs from males. Our results confirm a critical role of IC BK channels in FIKS. Sex contributes to the capacity for adaptation to a HK diet in IC-BKα–KO mice.

Introduction

Urinary K^+ secretion in the aldosterone-sensitive distal nephron (ASDN), including the late distal convoluted tubule (DCT), connecting tubule (CNT), and cortical collecting duct (CCD), is mediated by at least 2 K^+ secretory channels: a low-conductance renal outer medullary potassium (ROMK) channel (1–5) and a high-conductance Ca^{2+}-, voltage-, and stretch-activated BK channel (2, 6–13). Cumulative evidence now suggests that the ROMK channel mediates constitutive K^+ secretion, while the iberiotoxin-sensitive BK channel, composed of pore-forming α subunits (encoded by Slo1 or Kcnma1) and accessory β and γ subunits (14–16), is responsible for flow-induced K^+ secretion (FIKS) (13, 17–21).

Both ROMK and BK channels play major roles in the renal adaptation to dietary K^+ (17, 20, 22–24). Expression of ROMK is restricted to principal cells (PCs), cells with robust basolateral Na^+/K^+-ATPase activity that have traditionally been considered to mediate electrogenic epithelial Na^+ channel–dependent (ENaC-dependent) transepithelial Na^+ absorption and K^+ secretion (1–4). Conducting BK channels are detected in both PCs and acid-base transporting intercalated cells (ICs) in rat and rabbit ASDN (2, 8–10). Two major populations of ICs have been identified in the CCD. B-type ICs secrete HCO_3^- via the apical Cl^-/HCO_3^- exchanger pendrin and possess a basolateral H^+-ATPase, whereas A-type ICs secrete H^+ via an apical H^+-ATPase and a basolateral Cl^-/HCO_3^- exchanger similar to the red cell anion exchanger 1 (AE1) (25).

A major question — as yet unresolved, to our knowledge — is whether ICs and/or PCs mediate BK channel–mediated FIKS and/or K^+ adaptation in the ASDN. In support of a role for ICs in this process are the observations that (a) electrophysiologic (8–10, 26) and immunolocalization (23, 24, 27–29) studies reveal a higher density of BK channels in ICs versus PCs in the ASDN; (b) when rats are fed a high K^+ (HK) diet for as little as 18 hours, a significant fraction of K^+ excretion becomes amiloride insensitive and,

Authorship note: RCG and ECR contributed equally to this work.

Conflict of interest: TRK receives an honorarium from Wiley Inc. for serving as Editor of Physiological Reports.

Submitted: May 24, 2019
Accepted: March 25, 2020
Published: April 7, 2020.

Reference information: *JCI Insight*. 2020;5(8):e130553. https://doi.org/10.1172/jci.insight.130553.

thus, independent of ENaC, presumably reflecting the recruitment of a non–PC-mediated pathway for K^+ secretion into the urine (30); (c) dietary K^+ loading of rabbits leads to an increase in ICs of immunodetectable apical BKα and the long isoform of with-no-lysine kinase 1 (L-WNK1), a kinase that increases BKα abundance and functional channel expression in heterologous expression systems (31, 32); (d) the apical membrane of the IC is depolarized relative to that of the PC (26, 33, 34), suggesting that there exists a favorable driving force for K^+ efflux across this membrane; and (e) increases in tubular fluid flow rate lead to increases in the intracellular Ca^{2+} concentration ($[Ca^{2+}]_i$) in both ICs and PCs (35–37), and only a modest increase in $[Ca^{2+}]_i$ is necessary to open BK channels (26).

To directly address the role of ICs in BK channel–mediated renal regulation of K^+ homeostasis (FIKS and adaptation to dietary K^+) in the ASDN, we generated and characterized a mouse model with cell-specific targeted disruption of BKα, the pore-containing subunit of the BK channel, in ICs in the ASDN (IC-BKα–KO). The functional consequences of this gene disruption on BK channel activity were assessed in single ICs and PCs by measurement of charybdotoxin-sensitive (ChTX-sensitive) whole cell K^+ currents and in isolated microperfused CCDs by measurement of flow-stimulated K^+ transport. The impact of loss-of-function of IC BK channels on whole animal adaptation to a dietary K^+ load was examined by measuring blood $[K^+]$ and by assessing urinary K^+ clearance. We found a paucity of BK-dependent K^+ currents in ICs from HK-fed IC-BKα–KO mice, and microperfused CCDs from these mice lacked FIKS. Surprisingly, a higher blood $[K^+]$ was observed only in IC-BKα–KO male mice on a HK diet compared with controls — not female mice.

Results

Validation of the IC-specific disruption of BKα. B1-Cre mice conferred an IC-specific KO, as evidenced by IC- but not PC-specific Cre recombinase activity, in offspring of B1-Cre mice crossed with $ROSA26^{tdTomato}$ reporter mice, which express red fluorescent protein when a floxed Stop sequence is excised (Figure 1). IC-BKα–KO mice were born at a frequency slightly lower (20%) than expected but gained weight (Figure 2) and developed normally, were fertile, and had no gross morphologic abnormalities. PCR of DNA from kidney cortex revealed BKα gene recombination in KO mice (Figure 3).

ICs represent less than 30% of the cells present in the CCD and a very small subset of cells present in the cortex of the mouse kidney, and BK channels are present in both PCs and ICs of the CCD (24). In fact, we did not detect a difference in steady state abundance of BKα message in isolated CCDs (10–12.5 mm total length per sample) between floxed control and IC-BKα–KO mice by quantitative PCR (qPCR); the relative expression of BKα in CCDs from 3 KO versus 3 control mice was 1.4 ± 0.5 ($P = 0.18$).

Whole cell BK channel currents are dampened in IC-BKα–KO mice. Perforated whole cell recordings of K^+ currents were performed in ICs and PCs clamped at +60 mV in CCDs of floxed control and IC-BKα–KO mice (Figure 4). Based on the observation that ChTx (100 nM), a peptide inhibitor of BK channels (12, 13), inhibited whole cell K^+ currents in ICs in floxed mice fed a control K^+ (CK) diet (Figure 4A), the identity of these ChTX-sensitive currents was assigned as those mediated by BK channels. ChTX-sensitive currents in ICs, averaging 500 ± 65 pA/cell (mean ± SD) in CK-fed floxed control mice ($n = 4$), increased to 742 ± 33 pA/cell in these mice fed a HK diet ($n = 4$, $P < 0.03$; Figure 4E), similar to results reported previously (8). ChTX-sensitive current density in ICs in IC-BKα–KO CCDs, isolated from mice fed a HK diet for 10 days to maximize BK channel expression, was significantly less than observed in control littermates, averaging only 35 ± 12 pA/cell ($n = 10$, $P < 0.01$; Figure 4E). In contrast, ChTx-sensitive K^+ currents in PCs in CCDs from IC-BKα–KO mice fed a HK diet were greater than those in control HK-fed littermates (454 ± 40 versus 304 ± 28 pA/cell, $n = 6$ and 5, respectively, $P < 0.01$; Figure 4F).

In vitro microperfused CCDs isolated from IC-BKα–KO mice fail to exhibit FIKS. The impact of the cell-specific disruption of BKα on basal and flow-induced net K^+ secretion (JK) and Na^+ absorption (JNa) was studied in microperfused CCDs isolated from male and female mice fed a HK diet to maximize BK channel expression (23, 24). In CCDs from control mice ($n = 7$, including 4 males and 3 females), an increase in tubular fluid flow rate from 0.9 (slow) to 5.5 (fast) nL/min per mm was associated with a significant increase in JNa (from 7.7 ± 8.3 to 42.7 ± 9.6 pmol/min per mm; $P < 0.01$) and JK (from –1.6 ± 1.4 to –5.9 ± 1.6 pmol/min per mm; $P < 0.01$) (Figure 5, A and D). Analysis of sex-specific rates of transepithelial Na^+ and K^+ transport in control mice revealed no significant differences between males and females (Figure 5). In the 4 CCDs from the male controls, the increase in tubular fluid flow rate led to a significant increase in JNa (from 11.4 ± 9.8 to 43.3 ± 13.0 pmol/min per mm; $P < 0.01$) and JK (from –1.6 ± 1.0 to –5.0 ± 1.1

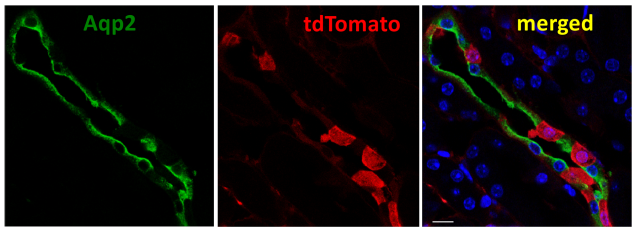

Figure 1. Specificity of Cre expression in B1-Cre mice crossed with ROSA26^{tdTomato}. Confocal microscopic examination of cryosections from offspring of these mice revealed that cells expressing the B1-Cre transgene did not colabel with an antibody directed against principal cell–specific AQP2, consistent with cell-specific Cre activity in intercalated but not principal cells in the CCD. Scale bar: 10 μM.

pmol/min per mm; $P < 0.01$) (Figures 5, B and E). In 3 CCDs from the female controls, the increase in tubular fluid flow rate led to a significant increase in JNa (from 2.9 ± 0.3 to 41.8 ± 4.7 pmol/min per mm; $P < 0.01$) and JK (from –1.5 ± 2.1 to –7.1 ± 1.5 pmol/min per mm; $P < 0.01$) (Figures 5, C and F).

In CCDs ($n = 9$) from IC-BKα–KO mice of both sexes, JNa was also stimulated in response to a 5-fold increase in luminal flow rate (8.2 ± 10.8 to 43.5 ± 29.7 pmol/min per mm; $P < 0.05$), an increase similar to that observed in control mice (Figure 5A). However, an increase in luminal flow rate failed to elicit FIKS in CCDs ($n = 8$) from IC-BKα–KO mice of both sexes (–0.7 ± 0.6 to –0.8 ± 1.4 pmol/min per mm) (Figure 5D). Analysis of sex-specific rates of transepithelial Na^+ transport revealed that flow-stimulated but not basal rates of net Na^+ absorption in female IC-BKα–KO mice exceeded that measured in males (Figures 5, B and C). In 6 CCDs from the male KOs, the increase in tubular fluid flow rate led to a significant increase in JNa (from 9.4 ± 12.2 to 26.9 ± 20.3 pmol/min per mm; $P < 0.01$), whereas JK was unchanged (–0.7 ± 0.5 to –1.1 ± 1.4 pmol/min per mm) (Figures 5, B and E). In 3 CCDs from the female KOs, the increase in tubular fluid flow rate led to a significant increase in JNa (from 5.8 ± 9.4 to 76.6 ± 6.3 pmol/min per mm; $P < 0.01$), whereas JK was unchanged (from –0.5 ± 0.8 to –0.1 ± 1.3 pmol/min per mm) (Figure 5, C and F). Flow-stimulated JNa in 3 female KOs was fully inhibited by 3 μM luminal benzamil, averaging 8.7 ± 6.0 pmol/min per mm (Figure 5C).

BK channel–mediated FIKS requires not only net Na^+ absorption, but also flow-induced increases in $[Ca^{2+}]_i$ sufficient to activate the channel (35). We thus sought to examine whether targeted disruption of BKα in IC-BKα–KO mice impacted the ability of luminal flow to trigger increases in $[Ca^{2+}]_i$. In CCDs from control mice ($n = 6$, including 3 males and 3 females), a rapid increase in tubular fluid flow rate led to a typical high-amplitude increase in the fura 2 fluorescence intensity ratio (FIR; ratio of emission signals measured at excitation wavelengths of 340 nm and 380 nm) — corresponding to $[Ca^{2+}]_i$ — in both PCs and ICs (Figure 6, A and B), followed by a gradual decay to a plateau value. As previously reported (36), the FIR remained significantly elevated above baseline for at least 20 minutes during a period of sustained high flow. Identical results were observed in PCs and ICs in CCDs isolated from IC-BKα–KO mice ($n = 6$, including 3 males and 3 females). Analysis of sex-specific flow-induced $[Ca^{2+}]_i$ responses in control and IC-BKα–KO mice revealed that peak and plateau elevations of FIR at 15, 30, and 60 seconds were greater in females ($n = 6$) than in males ($n = 6$, $P \leq 0.05$) (Figure 6C).

Effects of HK diet on blood [K^+] and urinary K^+ excretion. The impact of the genetic manipulations of BKα in ICs on whole blood [K^+] and on urinary K^+ (and Na^+) excretion was assessed in animals fed a HK diet for > 10 days. In response to initiating a HK diet, both IC-BKα–KO and littermate control mice consumed equivalent amounts of diet (Figure 7A) and lost weight to a similar degree (Figure 7B). Water consumption

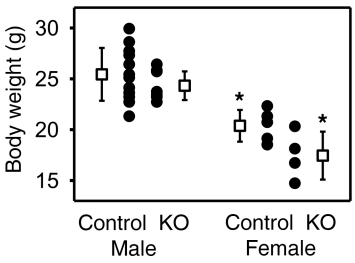

Figure 2. Body weights of 12- to 14-week-old floxed control and IC-BKα–KO mice fed a HK diet for 10 days. Male control ($n = 12$) and IC-BKα–KO ($n = 8$) mice reached a greater weight than did females ($n = 5$ controls and 4 KOs), although there was no significant difference between control and KO mice of a given sex. Individual data points, as well as mean ± SD (box with SD bars) are shown for each group. *$P < 0.01$ compared with males of the same genotype, 2-tailed unpaired Student's *t* test.

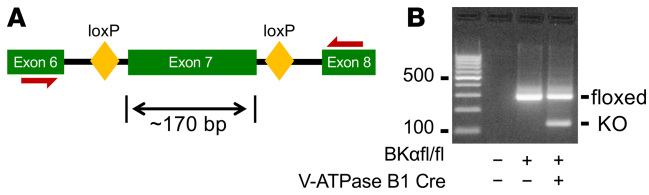

Figure 3. Generation of floxed BKα allele and targeted deletion of BKα in intercalated cells. (**A**) Schematic representation of floxed allele showing LoxP sites flanking exon 7 of Kcnma1. (**B**) Representative blot of PCR products from renal cortex of BKα$^{fl/fl}$ mice and BKα$^{fl/fl}$ mice bred with B1-Cre mice using nested BKα-specific primers. Genotyping revealed a band at 132 bp in the IC-BKα–KO mouse, reflecting Cre-mediated excision of the BKα pore domain in BKα$^{fl/fl}$ mice. The upper 306-bp band is the uncombined allele.

and urine volume increased significantly in both IC-BKα–KO and control mice following the transition to a HK diet (Figures 7, C and D; $P < 0.001$). Daily net urinary Na^+ excretion changed significantly as a function of time (Figure 7E, $P < 0.001$). There was no difference between genotypes. However, as independent variables influencing Na^+ excretion, genotype and time interacted significantly ($P = 0.004$). Net urinary K^+ excretion significantly increased in both groups following the transition to the HK diet, as expected (Figure 7F, $P < 0.001$). There was no difference between genotypes and no evidence that time and genotype interacted in influencing K^+ excretion. At day 5 on the HK diet, blood [K^+] concentrations were similar ($P = 0.43$ by 1-way ANOVA) in IC-BKα–KO males (5.1 ± 0.9 mEq/L, $n = 8$), IC-BKα–KO females (5.0 ± 0.7 mEq/L, $n = 4$), control males (5.6 ± 0.8 mEq/L, $n = 7$), and control females (4.9 ± 0.7 mEq/L, $n = 4$). However, at day 13 on the HK diet, IC-BKα–KO mice exhibited significantly higher blood [K^+] (5.5 ± 0.8 mEq/L, $n = 21$) than littermate controls (5.0 ± 0.7, $n = 24$, $P < 0.05$; Table 1 and Figure 8). Surprisingly, male and female mice differed with regard to changes in blood [K^+] in response to the HK diet. While IC-BKα–KO male mice had significantly higher blood [K^+] (5.7 ± 0.7 mEq/L, $n = 14$) than controls (5.0 ± 0.7 mEq/L, $n = 16$, $P < 0.05$), differences were not observed in female mice (5.1 ± 0.8 mEq/L, $n = 7$, IC-BKα–KO; 5.0 ± 0.8 mEq/L, $n = 8$, control). There were no significant differences in blood [Na^+] (Figure 8) or total CO_2 (Table 1) between male and female IC-BKα–KO and control mice.

To examine whether disruption of BKα influenced flow-induced K^+ excretion in mice on a HK diet, animals were injected with an isotonic saline bolus, and urine was collected over the subsequent 6 hours to measure urinary electrolyte excretion. No differences in urinary volume or osmolality were observed among IC-BKα–KO and control male and female mice, and differences were not detected in the rate of urinary Na^+ excretion ($U_{Na}V$), the rate of urinary K^+ excretion (U_KV), and the ratio of urinary Na^+ to K^+ excretion (U_{Na}/U_K) (Table 2).

Given the differences in blood [K^+] observed between IC-BKα–KO and control mice on a HK diet, we asked whether aldosterone levels differed between these groups. Circulating levels of plasma aldosterone were elevated in HK-fed mice (Table 3) compared with values reported by others in C57BL/6J mice fed a standard K^+ diet (less than 500 pg/mL), as expected (38, 39). There were no significant differences in plasma aldosterone levels detected between IC-BKα–KO mice and controls (Table 3).

BKα expression is enhanced in DCT of IC-BKα–KO mice. Given the preservation of urinary K^+ excretion in IC-BKα–KO mice on a HK diet (Figure 7) — or following volume expansion (Table 2) — and the absence of detectable FIKS in microperfused CCDs isolated from HK-fed KO mice (Figure 5), we sought to examine whether BKα expression was upregulated in segments upstream from the CCD. The inability to precisely distinguish the CNT, the primary segment responsible for urinary K^+ secretion (40, 41), from the CCD — both of which are composed of cells expressing identical repertoires of transport proteins — led us to examine adaptation of the DCT to downstream loss of BKα. In kidney sections prepared from floxed control and IC-BKα–KO mice ($n = 3$ for each genotype), co–immunolabeled side-by-side with antibodies directed against DCT-specific NCC and BKα, we observed that relative BKα apical + subapical expression in NCC-expressing cells was significantly greater in IC-BKα–KO mice (1.6 ± 0.3) than in littermate controls (1.0 ± 0.2; $P < 0.001$) (Figure 9).

Discussion

This study aimed to examine the contribution of the IC BK channel to the renal adaptation to dietary K^+ loading and FIKS in the setting of a HK diet. To this end, we generated IC-BKα–KO mice by crossing floxed BKα mice with B1 H^+-ATPase Cre mice, after confirming that the B1 Cre was expressed primarily in

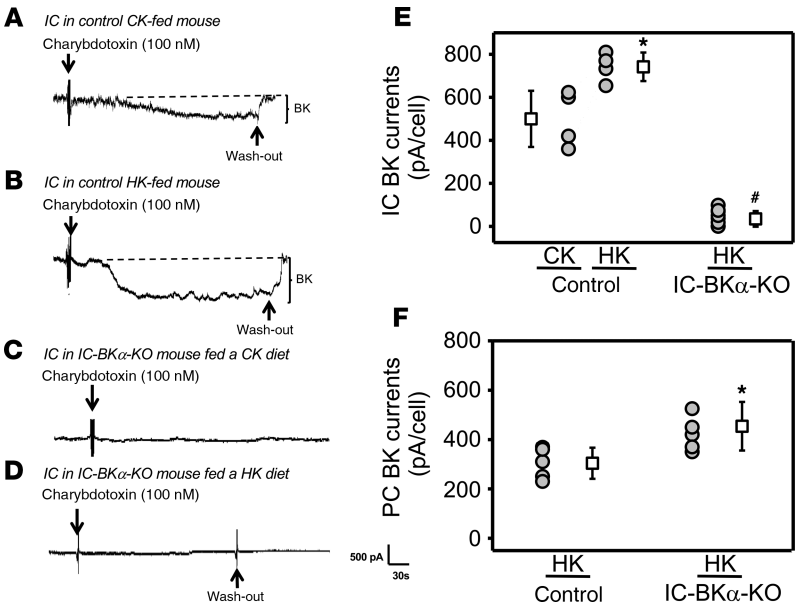

Figure 4. Perforated whole cell patch recordings of charybdotoxin-sensitive (ChTx-sensitive) currents in intercalated cells (ICs) and principal cells (PCs) in CCDs from IC-BKα–KO and floxed control mice. Recordings were performed in cells clamped at +60 mV. The composition of the bath and pipette solutions, which both contained 130 mM K-gluconate, is given in Methods. Currents were normalized to a membrane capacitance of 13 pF per cell. (**A–D**) Representative current tracings are shown on the left for ICs in CCDs isolated from floxed control K^+–fed (CK-fed) (**A**), floxed high K^+–fed (HK-fed) (**B**), KO CK-fed (**C**), and KO HK–fed mice (**D**). (**E**) Summary graph showing individual data points and mean ± SD (box with SD bars) for ChTx-sensitive current density in ICs in floxed mice fed a CK diet (n = 4 ICs), averaging 500 ± 65 pA/cell, enhanced to 742 ± 33 pA/cell (n = 4 ICs, $P < 0.03$) in mice fed a HK diet for 10 days to maximize BK channel expression. BK channel activity in ICs in IC-BKα–KO CCDs isolated from mice fed a HK diet (n = 10 ICs) was minimal. *$P < 0.05$ compared with CK-fed controls and #$P < 0.05$ compared with HK-fed controls, 2-tailed unpaired Student's t test. (**F**) Summary graph as described for **E** showing ChTx-sensitive currents in PCs in CCDs from HK-fed IC-BKα–KO mice (n = 6 PCs); these currents were greater than those in HK-fed floxed littermates (n = 5 PCs). *$P < 0.05$ compared to HK-fed controls, 2-tailed unpaired Student's t test. Data were obtained from both male and female mice.

ICs in the kidney (Figure 1). While we were unable to demonstrate unequivocal evidence of IC-specific loss of message and protein in ICs in the IC-BKα–KO mice, targeted disruption of BKα in HK-fed IC-BKα–KO mice led to a dramatic reduction in whole cell ChTX-sensitive K^+ currents in ICs (Figure 4). We noted a modest upregulation of these currents in PCs when compared with floxed controls, an observation we speculate reflects a compensatory response to the loss of BK channels in adjacent ICs. Microperfused CCDs isolated from HK-fed control and IC-BKα–KO mice exhibited baseline JK and JNa (Figure 5). Disruption of BKα in ICs led to the loss of FIKS in microperfused CCDs isolated from HK-fed male and female IC-BKα–KO mice, and it enhanced benzamil-sensitive and, thus, ENaC-mediated flow-stimulated Na^+ absorption in females; however, it did not affect flow-induced $[Ca^{2+}]_i$ transients in either sex (Figure 5 and Figure 6). These observations underscore the critical role of IC BK channels in mediating FIKS.

We examined the impact of a loss of IC BK channel expression on whole animal adaptation to a HK diet. Blood $[K^+]$ in IC-BKα–KO mice significantly exceeded that measured in controls after 13 days on a HK diet (Table 1 and Figure 8). This increase in blood $[K^+]$ was only seen in males. We did not detect a difference in blood $[K^+]$ between IC-BKα–KO and controls when mice were on a HK diet for only 5 days. Our observations of preserved urinary K^+ excretion in IC-BKα–KO mice on a HK diet, whether assessed daily (Figure 7) or following volume expansion (Table 2), and the absence of detectable FIKS in the isolated microperfused CCD (Figure 5) implies that alternate K^+ secretory processes are upregulated in this discrete segment or others (e.g., the DCT or CNT) in the absence of conducting IC BK channels and are recruited to secrete K^+ under conditions of dietary K^+ loading and high urinary flow. Indeed, we demonstrated upregulation of immunodetectable BKα in the DCT of HK-fed IC-BKα–KO mice compared with floxed littermates (Figure 9).

There exists considerable evidence for sex-specific differences in the renal regulation of ion homeostasis. Sexual dimorphism in renal K^+ handling on a HK diet has been noted in rats, with females (versus males) exhibiting a higher urinary $[K^+]$, proposed to be due to lower fractional reabsorption of Na^+ in the proximal

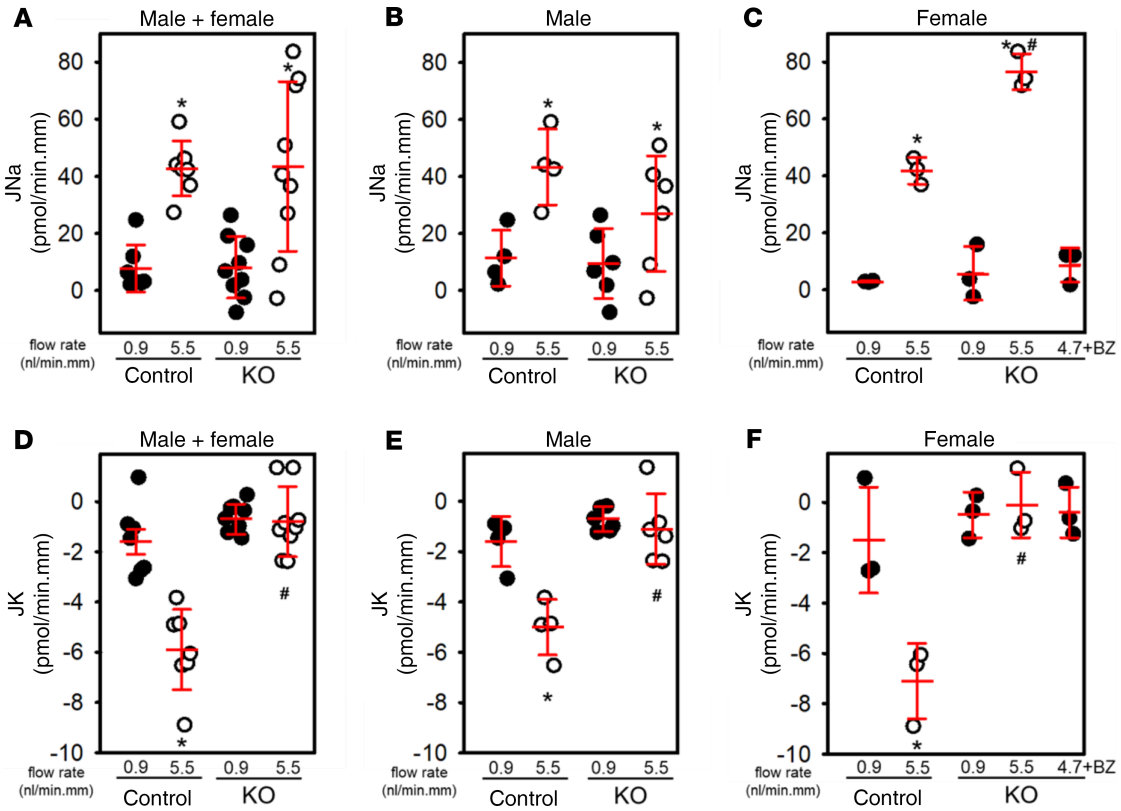

Figure 5. Basal and flow-induced net Na absorption (JNa) and K secretion (JK) in microperfused CCDs isolated from HK-fed IC-BKα–KO and control floxed mice. (**A** and **D**) In 7 CCDs from control mice (4 male and 3 female), an increase in tubular fluid flow rate from 0.9 (slow, closed circle) to 5.5 (fast, open circle) nL/min per mm was associated with a significant increase in JNa (**A**) and JK (**D**). Basal and flow-stimulated JNa were similar in CCDs from these control and 9 IC-BKα–KO mice (6 male and 3 female). (**E** and **F**) However, flow-induced K^+ secretion (FIKS) was absent in CCDs from IC-BKα–KO male (**E**) and female (**F**) mice. (**B** and **C**) Flow-stimulated but not basal rates of transepithelial Na^+ transport in female IC-BKα–KO mice (**C**) exceeded that measured in males (**B**) and was inhibited by 3 μM benzamil (BZ, $n = 3$). Mean ± SD. $^*P < 0.05$ compared with JNa or JK at 0.9 nL/min per mm in same tubules, by 2-tailed paired Student's *t* test; $^{\#}P < 0.05$ compared with JNa or JK in control tubules studied at same flow rate, by 2-tailed unpaired Student's *t* test.

nephron leading to increased distal Na^+ delivery and K^+ secretion, as well as a lower baseline plasma [K^+] (42). The authors further noted that the distal nephron of the female versus male rat had higher abundance of cleaved ENaC α and γ subunits (42), a finding that may provide insight into the enhanced flow-stimulated Na^+ absorption detected in female versus male IC-BKα–KO mice (Figure 5). No sexual dimorphism in ROMK abundance was evident in rats fed a control or a single 2% K^+-rich meal (42). Another study reported sex-dependent differences in kidney expression of both BKα and WNK1 protein in C57BL/6 mice (43). Although higher levels of expression of both proteins were detected in kidney homogenates prepared from female versus male mice fed a standard K^+ diet, sex-dependent differences were eliminated when mice were fed a HK diet (43). BKα and WNK1 are expressed in multiple cell types in the kidney, and our study highlights the importance of examining cell-specific expression of these proteins. Differences in levels of BK channel expression, based on sex, have also been described in other organs (44, 45).

We speculate that the sex differences we observed are due to differences in circulating levels of sex hormones, which change during postnatal development and in females, throughout estrus cycle and pregnancy (46, 47). Sex differences may also be due to the sex chromosome complement (XX versus XY) (48, 49). Gonadal hormones regulate expression, composition, and activity of ENaC in a variety of tissues and cultured CCD cells (50–52), as well as urinary K^+ excretion and renal K^+ channel expression and activity (43, 53–56). The physiologic basis for and mechanisms underlying sex differences in the regulation of K^+ homeostasis under basal and K^+-adapted conditions remain to be elucidated. Future efforts must extend to assessment of sex differences in the capacity of not only the kidney, but also the gut for regulation of K^+ transport.

The mild phenotype of the IC-BKα–KO mouse was not surprising, given previous developmental studies demonstrating that the weanling rabbit (<30 days) is essentially a BKα-KO model (21). BKα mRNA transcript expression is not detected until the fourth week of life in rabbits, a brief time interval

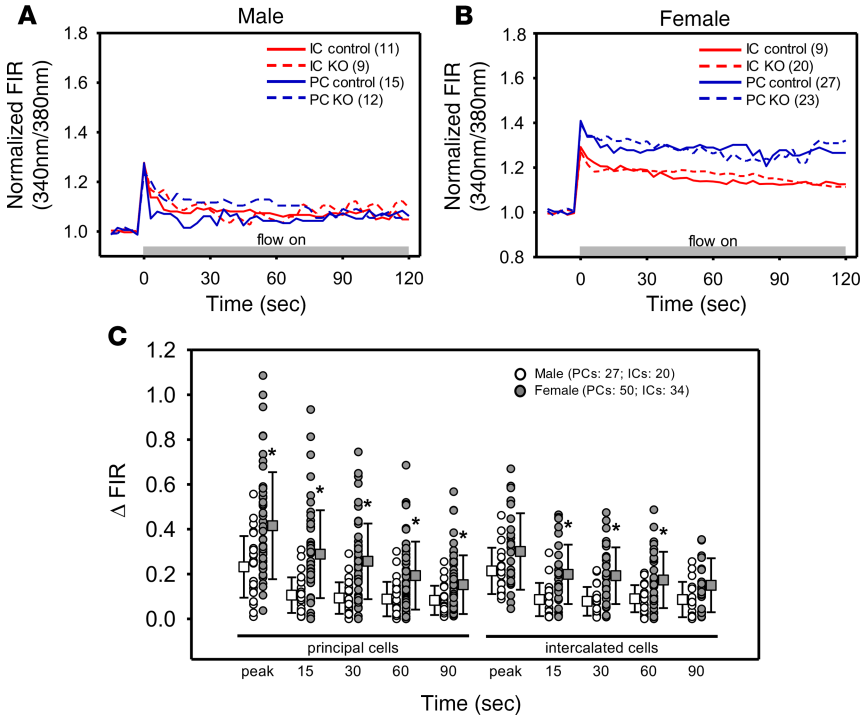

Figure 6. Effect of targeted deletion of BKα in intercalated cells on flow-induced increases in fura 2 fluorescence intensity ratio (FIR), a measure of intracellular Ca^{2+} concentration ($[Ca^{2+}]_i$), in microperfused CCDs. (**A** and **B**) Summary tracings, representing the average fura 2 FIRs recorded in individual cells (number of cells in parentheses in 3 CCDs per genotype) prior to and following an acute increase in flow rate. The FIR in intercalated (IC, red) and principal (PC, blue) cells in fura 2–loaded CCDs isolated from male (**A**) and female (**B**) floxed control (solid lines) and IC-BKα–KO (dashed lines) mice were normalized to the FIR measured immediately prior to the increase in flow rate. An acute increase in luminal flow rate led to a typical biphasic response including an immediate rapid increase in FIR to a peak value within ~10 seconds, presumably secondary to basolateral Ca^{2+} entry and release of Ca^{2+} from internal stores, followed by a gradual decay to a plateau value that exceeds baseline for at least 120 seconds of sustained high flow. The latter plateau elevation in FIR is believed to represent mechano-induced Ca^{2+} influx into cells. No significant differences in the immediate peak response or the plateau elevation in FIR were detected in each individual cell type between control and IC-BKα–KO mice. (**C**) Data were thus pooled; graph presents the change in FIR from baseline of all cells studied in male (open circle) and female (closed circle) mice at intervals following an acute increase in flow rate. The elevation of FIR at 15, 30, 60 and 90 seconds after high flow was initiated was greater in females (n = 6 mice) compared males (n = 6 mice, $P \le 0.05$). Number of cells studied in 3 CCDs per genotype is given in parentheses. Mean ± SD. *$P < 0.05$ female versus male at specific times (sec), 2-tailed unpaired Student's t test.

marked by a 6-fold increase in consumption of pelleted food and precipitous fall in milk intake (57). Immunodetectable BKα protein is first evident during the fifth week of postnatal life, the age at which FIKS can first be detected in microperfused CCDs (21). The absence of FIKS early in life is not limited by the capacity of the CCD to respond to an increase in flow with augmented Na^+ absorption or a rise in $[Ca^{2+}]_i$ (21). In fact, the transport and signaling pathways mediating the latter mechano-induced responses appear to be established at an early age (21).

The results of the current study challenge the paradigm that PCs are the primary K^+ secretory cell in the ASDN. Our data provide compelling evidence that ICs, cells not traditionally considered to participate in renal K^+ secretion, are capable of secreting K^+ into the urinary fluid under conditions of dietary K^+ loading and high flow. As the B1 Cre transgene targets both A-type and B-type ICs (58), we are unable to identify the specific IC populations responsible for FIKS and K^+ adaptation. However, our previous observations that a HK diet leads to an increase in apical BKα expression in pendrin-expressing ICs (24), as well as cells expressing luminal H^+-ATPase (23), suggests that both IC subtypes participate in K^+ adaptation.

We recently reported that immunoreactive BKα is abundant in the apical central cilium of PCs in rabbit CCD, where it colocalizes with the β1 subunit, and that deciliation of CCDs does not dampen FIKS (24).

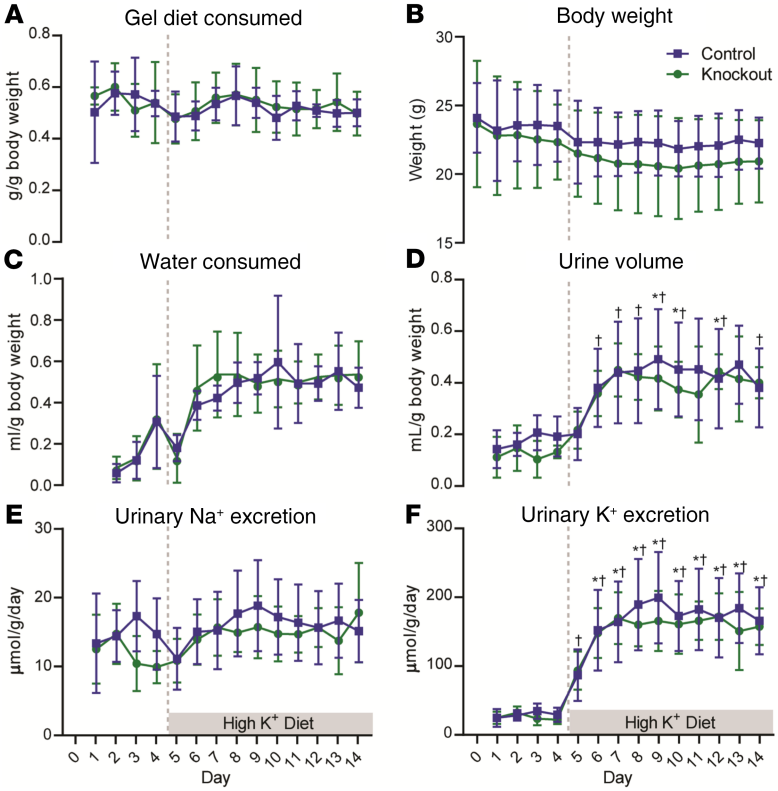

Figure 7. Urine electrolyte and other parameters measured in response to the HK diet. IC-BKα–KO (n = 6; 3 female and 3 male) and floxed control (n = 6; 3 female and 3 male) mice were placed in metabolic cages for 4 days on a control diet. Their diet was then transitioned to HK (5% K as KCl) for 10 days of monitoring. (**A–F**) Diet consumed (**A**), mouse body weight (**B**), water consumed (**C**), urine volume (**D**), daily urine Na^+ excretion (**E**), and urine K^+ excretion (**F**) (all normalized to mouse weight) are shown. In mixed effects analysis, there was a statistically significant change over time ($P < 0.001$) in all parameters except diet consumed. There were no significant differences between genotypes. Urine Na^+ excretion exhibited statistically significant interaction between day and genotype ($P = 0.004$). Values significantly different from baseline before HK diet (day 4) are marked for IC-BKα–KO mice ($^{\dagger}P < 0.05$) or control mice ($^{*}P < 0.05$).

These observations led us to conclude that the cilia BKα/β1 channel does not participate in K^+ secretion. As disruption of BKα in ICs completely abolishes FIKS in isolated CCDs and impairs K^+ adaptation, the role of the apical BK channel in PCs remains to be defined.

ICs in mouse CNT and CCD have been reported to express β4 subunit (28), a subunit that renders BKα resistant to low nM concentrations of iberiotoxin (59, 60). Mice lacking BKβ4 have no detectable phenotype under baseline conditions when fed a normal diet but demonstrate an impaired kaliuresis in response to dietary K^+ loading (61). As the focus of this investigation was on BKα, we did not examine the expression and localization of discrete β subunits.

In sum, the results of the current investigation provide compelling evidence for the critical role of IC BKα in BK channel–mediated K^+ secretion, activated by dietary K^+ loading and increases in tubular fluid flow. Our identification of ICs as K^+ secretory cells challenges the primacy of PCs as the sole K^+ secretory cell in the distal nephron and adds to the ever-expanding repertoire of transport and other cellular functions ascribed to ICs (62–64).

Table 1. Blood values after 13 days on high K^+ diet

	Genotype	All mice	Female	Male
Na^+ (mEq/L)	Control	144 ± 3 (n = 24)	143 ± 5 (n = 8)	145 ± 2 (n = 16)
	IC-BKα–KO	146 ± 3 (n = 21)	146 ± 4 (n = 7)	146 ± 3 (n = 14)
K^+ (mEq/L)	Control	5.0 ± 0.7 (n = 24)	5.0 ± 0.8 (n = 8)	5.0 ± 0.7 (n = 16)
	IC-BKα–KO	5.5 ± 0.8 (n = 21)^{A}	5.1 ± 0.8 (n = 7)	5.7 ± 0.7 (n = 14)^{A}
tCO_2 (mM)	Control	21 ± 3 (n = 24)	21 ± 4 (n = 8)	21 ± 3 (n = 16)
	IC BKα-KO	22 ± 2 (n = 21)	20 ± 2 (n = 7)	23 ± 2 (n = 14)

Mean ± SD (number of mice). $^{A}P < 0.05$, control versus IC-BKα–KO mice by 2-tailed unpaired Student's t test. tCO_2, total CO_2.

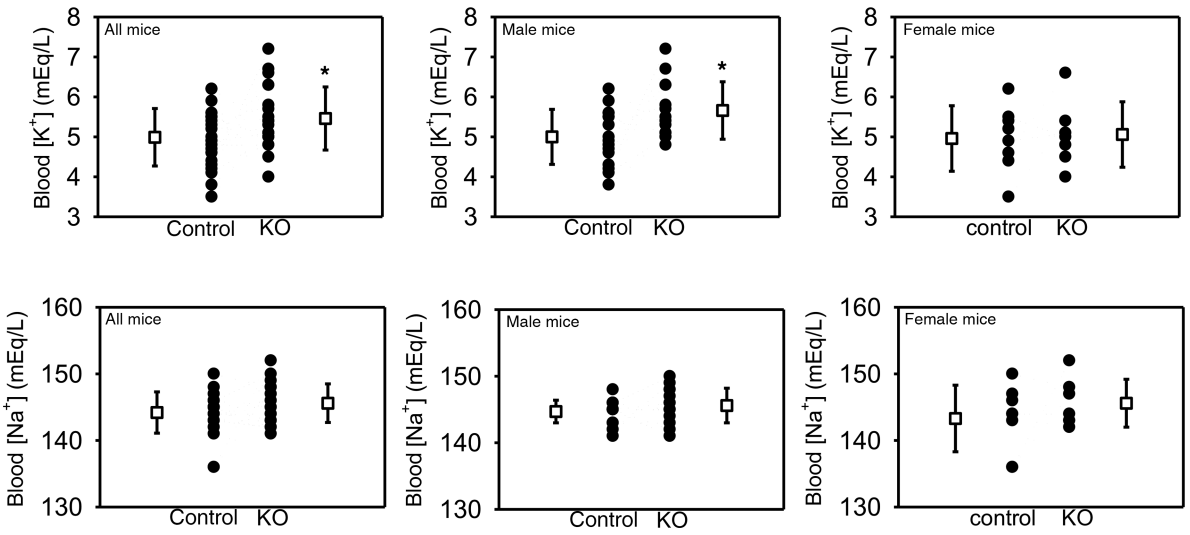

Figure 8. Whole blood electrolytes in HK-fed IC-BKα–KO and floxed control mice. IC-BKα–KO and floxed control mice were maintained on a HK diet for 13 days, and whole blood [K^+] and [Na^+] were subsequently determined. Individual data points, as well as mean ± SD (box with SD bars), are shown. Results for all animals, as well as results segregated by sex, are shown. *$P < 0.05$ versus floxed controls, by 2-tailed unpaired Student's *t* test. *n* = 24 floxed control mice including 16 males and 8 females; *n* = 21 IC-BKα–KO mice including 14 males and 7 females.

Methods

Animals. Mice were allowed free access to tap water and chow. Mice were provided a 1% CK (Envigo Teklad, TD.88238) diet at the time of weaning and were then switched to a 5.2% K^+ (provided as KCl, HK; Envigo Teklad, TD.09075) diet 10 days before study to maximally stimulate BK channel expression, unless otherwise indicated. All diets contained 0.3% Na^+.

Generation of BKα floxed mice. Based on the presence in exon 7 of the BKα gene of both the S6 domain and the P loop with the selectivity filter within the pore region, a targeting construct was made containing 3 kb of flanking homologous DNA, a flippase recognition target–flanked (FRT-flanked) PGK promoter-Neo^R sequence, and 2 loxP sites surrounding this exon. The predicted 57–amino acid deletion in the protein does not introduce a frame shift or Stop codon, and disruption of exon 7 causes complete loss of BK channel activity (65). Thymidine kinase sequences were placed on either end of the vector.

Mouse SVJ129 embryonic stem cells (from the Transgenic Core at the University of Utah) were electroporated with the vector. Several BKα ES clones were screened by PCR analysis, and their identity confirmed by Southern analysis. One clone with a normal karyotype was identified, and this was used to inject into recipient C57BL/6J blastocysts. Founder agouti mice were obtained from the Jackson Laboratory, bred to

Table 2. Urine values

	Genotype	All mice	Females	Males
Urine volume (μL/6 hr)	Control	1520 ± 480 (*n* = 20)	1310 ± 590 (*n* = 7)	1640 ± 390 (*n* = 13)
	IC-BKα–KO	1560 ± 660 (*n* = 11)	820 ± 240 (*n* = 3)	1830 ± 530 (*n* = 8)
Osmolality (mOsm/kg)	Control	549 ± 88 (*n* = 20)	527 ± 88 (*n* = 7)	561 ± 90 (*n* = 13)
	IC-BKα–KO	562 ± 58 (*n* = 11)	593 ± 50 (*n* = 3)	551 ± 59 (*n* = 8)
$U_{Na}V$ (μmol/g/hr)	Control	1.41 ± 0.66 (*n* = 20)	1.57 ± 0.90 (*n* = 7)	1.33 ± 0.52 (*n* = 13)
	IC-BKα–KO	1.62 ± 0.62 (*n* = 11)	1.58 ± 0.96 (*n* = 3)	1.64 ± 0.54 (*n* = 8)
U_KV (μmol/g/hr)	Control	1.09 ± 0.48 (*n* = 20)	0.92 ± 0.36 (*n* = 7)	1.17 ± 0.52 (*n* = 13)
	IC-BKα–KO	1.15 ± 0.47 (*n* = 11)	1.13 ± 0.7 (*n* = 3)	1.15 ± 0.41 (*n* = 8)
U_{Na}/U_K	Control	1.37 ± 0.44 (*n* = 20)	1.61 ± 0.45 (*n* = 7)	1.24 ± 0.39 (*n* = 13)
	IC-BKα–KO	1.45 ± 0.37 (*n* = 11)	1.40 ± 0.12 (*n* = 3)	1.46 ± 0.44 (*n* = 8)

Mean ± SD (number of mice). Statistical differences were not observed between control and IC-BKα–KO mice by 2-tailed unpaired Student's *t* test.

Table 3. Aldosterone levels

	Controls	IC-BKα–KO
All	832 ± 544 (*n* = 19)	900 ± 587 (*n* = 17)
Female	927 ± 888 (*n* = 6)	839 ± 772 (*n* = 7)
Male	852 ± 336 (*n* = 13)	944 ± 459 (*n* = 10)

Aldosterone levels (pg/mL) were measured in plasma obtained from WT and IC-BKα–KO mice on a HK diet for 13 days. Mean ± SD (number of mice). Statistical differences were not observed between control and IC-BKα–KO mice by 2-tailed unpaired Student's *t* test.

C57BL/6J mice, and assessed for germline transmission of the floxed allele by tail vein clipping and genotyping. These mice were then bred with mice expressing Flp recombinase to excise the FRT-flanked PGK promoter-Neo^{R} cassette. Pups were analyzed for excision of the cassette, and the desired genotype was bred with C57BL/6J WT mice to eliminate Flp recombinase.

Generation of IC-BKα–KO mice. C57BL/6J mice expressing Cre recombinase under the control of the promoter of the B1 subunit of the H^+-ATPase (B1-Cre) (58) were used to generate an IC-specific KO. B1-Cre expression was confirmed by PCR amplification of the transgene using DNA isolated from tail biopsies, prepared by standard methods, and the following primers specific for Cre recombinase that yielded a 580 bp product: (Cre forward) 5′-CCCTCTTCCCTTCTCCCTCCA-3′ and (Cre reverse) 5′-GCGAACATCTTCAGGTTCTGCGG-3′.

To confirm cell-specific Cre expression, mice hemizygous for Cre recombinase were crossed with Rosa26^{tdTomato} reporter mice. Colabeling of cryosections of kidney cortex prepared from these animals was performed with a polyclonal goat anti-AQP2 antibody (0.2 μg/μL, sc-9882; Santa Cruz Biotechnology Inc.) and detected using a donkey anti–goat IgG conjugated to Cyanine Cy3 (0.5 μg/μL, Jackson ImmunoResearch). Images were acquired with a Leica TCS SP5 confocal microscope.

Male homozygous floxed BKα mice were bred with female B1-Cre–expressing mice. Female offspring hemizygous for B1-Cre and heterozygous for floxed BKα were bred with male homozygous floxed BKα mice to obtain mice homozygous for floxed BKα and hemizygous for B1-Cre (termed IC-BKα–KO). Subsequent colony expansion was achieved by crossing female KO with male homozygous floxed BKα mice. Sex-matched littermates that were homozygous for the floxed BKα genes, but without Cre, were used as controls in all studies. Body weights of 12- to 14-week-old IC-BKα–KO mice and floxed sex-matched littermates subjected to metabolic clearance studies were similar, although males weighed more than females (Figure 2). Mice of both sexes were used for all studies.

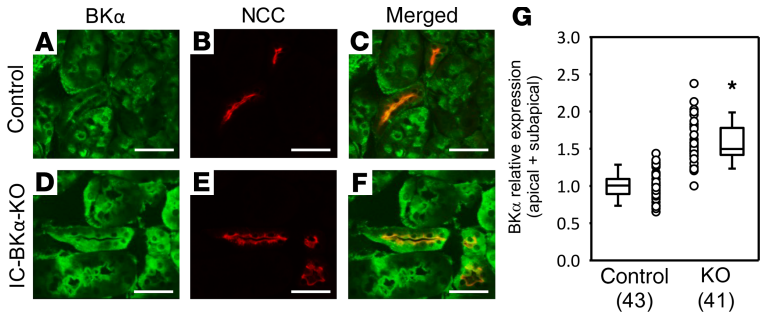

Figure 9. Immunodetectable apical BKα is more abundant in the DCT of IC-BKα–KO versus floxed control mice fed a HK diet for 10 days. Colabeling for BKα (**A** and **D**) and NCC (**B** and **E**) was performed in fixed kidney slices from HK-fed floxed control (**A–C**) and IC-BKα–KO (**D–F**) mice using antibodies directed against BKα (green; **A** and **D**) and NCC (red; **B** and **E**) to identify the DCT. The merged images (**C** and **F**) reveal BKα colocalization with NCC in the apical and subapical domains of DCT cells in control (**C**) and IC-BKα–KO (**F**) mice. Scale bars: 40 μm. (**G**) The mean fluorescence intensity (MFI) of BKα was measured in the apical + subapical region (defined by NCC labeling) of individually identified cells, captured in profile, in sections from 3 mice of each genotype. MFIs in the IC-BKα–KO (41 cells in 9 tubules) were normalized to the average of that measured in the floxed control (43 cells in 11 tubules). Analysis revealed that apical + subapical BKα abundance was 57% greater in IC-BKα–KO than control DCT. Individual data points, as well as median ± quartiles, are shown. *$P < 0.001$, by Mann-Whitney *U* test.

Genotyping was performed prior to weaning by PCR amplification of the floxed genomic region, using tail-derived DNA amplified with primers flanking the lox P sites: (forward) 5′-GCTTTGGATTCAGGCTGTAG-3′ and (reverse) 5′-GGCATGATTCACCAGAAACC-3′. The anticipated sizes of the products were 208 bp for the WT and 242 bp for the floxed alleles. RNA was extracted from kidney cortex and subject to reverse transcription PCR (RT-PCR) using external (e) and internal (i) nested primers to demonstrate BKα gene recombination. The external primers were: (eBKα forward) 5′-AGCTGGTGAATCTGCTCTCC-3′ and (eBKα reverse) 5′-CCCGGTCCTTGTGCAG-3′. The internal nested primers were: (iBKα forward) 5′-TGCTCTCCATATTTATCAGCACG-3′ and (iBKα reverse) 5′-AGGAGCCCCCGTATTTCTTG-3′. The anticipated product size was 306 bp in the floxed and 132 bp in the KO. PCR products were visualized after electrophoresis with 2% agarose.

Electrophysiologic analyses of BK channel currents. CCDs were isolated and split open. Perforated whole cell K^+ currents, recorded using an Axon 200A patch-clamp amplifier, were low-pass filtered at 1 KHz and digitized by an Axon interface (Digidata 1440A, Molecular Devices) (66, 67). Data were analyzed using the pCLAMP Software System 9 (Molecular Devices). Currents were measured using a bath solution containing (in mM): 130 K^+-gluconate, 10 KCl, 0.5 $MgCl_2$, 1.5 $CaCl_2$, and 10 HEPES (pH 7.4 with KOH). The pipette solution contained (in mM): 130 K^+-gluconate, 10 KCl, 1 $MgCl_2$, 8.72 $CaCl_2$, 10 EGTA (1 μM free Ca^{2+}), and 5 HEPES (pH 7.4 with KOH). After forming a high-resistance seal (>2 GΩ), the membrane capacitance was monitored until the whole cell patch configuration was formed. The IC and PC membrane capacitances were very similar, ranging between 12.5 and 13.5 pF; currents were normalized to a membrane capacitance of 13 pF per cell. The cells were clamped at +60 mV, and outward BK currents were identified by adding 100 nM ChTx to the bath solution.

In vitro microperfusion of isolated CCDs. In vitro microperfusion studies were performed using standard methodology, as previously described (13, 21, 68) and briefly summarized as follows. A single kidney was immediately excised after death of the animal, and coronal sections were placed in chilled dissection solution containing (in mM): 145 NaCl, 2.5 K_2HPO_4, 2.0 $CaCl_2$, 1.2 $MgSO_4$, 4.0 Na lactate, 1.0 Na citrate, 6.0 L-alanine, and 5.5 glucose (pH 7.4, 290 ± 2 mOsm/kg). Single CCDs (0.2–0.4 mm) were isolated by freehand dissection. A single tubule was studied from each mouse. Each isolated tubule was transferred to a temperature- and O_2/CO_2-controlled specimen chamber, placed on the stage of an inverted microscope (Nikon Eclipse), mounted on concentric glass pipettes, and perfused and bathed at 37°C with Burg's solution containing (in mM): 120 NaCl, 25 $NaHCO_3$, 2.5 K_2HPO_4, 2.0 $CaCl_2$, 1.2 $MgSO_4$, 4.0 Na lactate, 1.0 Na_3 citrate, 6.0 L-alanine, and 5.5 D-glucose (pH 7.4, 290 ± 2 mOsm/kg). The sequence of luminal flow rates in the 16 tubules studied was randomized between slow (0.9 ± 0.2 nL/min per mm) and fast (5.5 ± 0.8 nL/min per mm) to minimize any bias induced by time-dependent changes in ion transport. During the 45-minute equilibration period and thereafter, the perfusion chamber was continuously suffused with a gas mixture of 95% O_2–5% CO_2 to maintain pH of the Burg's solution at 7.4 at 37°C. The bathing solution was continuously exchanged at a rate of 10 mL/hour using a syringe pump (Razel Scientific). For selected tubules, 3 μM benzamil (Sigma-Aldrich, catalog B2417) was added to the perfusate to inhibit ENaC.

Measurements of net transepithelial cation transport. After equilibration, 3–4 samples of tubular fluid were collected under water-saturated light mineral oil by timed filling of a calibrated, approximately 10 nL volumetric constriction pipette under each experimental condition. Each tubule was perfused at both a slow (~0.9 nL/min per mm) and fast (~5.5 nL/min per mm) flow rates. The flow rate was varied by adjusting the height of the perfusate reservoir. The sequence of flow rates was randomized to minimize any bias induced by time-dependent changes in ion transport.

Finally, ouabain (200 μM, MilliporeSigma, catalog 4995) was added to the bath to inhibit all active transport, and an additional 3 samples of tubular fluid were obtained for analysis to determine the composition of the solution actually delivered to the lumen of the tubule. Both Na^+ and K^+ concentrations of perfusate and collected tubular fluid were determined by helium glow photometry, and the rates of net ion transport were calculated using standard flux equations, as previously described (27). As transport measurements were performed in the absence of transepithelial osmotic gradients and arginine vasopressin (AVP), water transport was assumed to be zero. The calculated ion fluxes were averaged to obtain a single mean rate of transport for the tubule under each experimental condition.

Assessment of flow-induced changes in $[Ca^{2+}]_i$. Isolated CCDs were transferred to the specimen chamber assembled with a No. 1 coverslip (Corning, catalog 2975225) painted with a 1 μL drop of poly-D-lysine hydrobromide 0.01% (BD Biosciences), set on the stage of the Nikon Eclipse TE 300 inverted epifluorescence microscope

linked to a Zyla 4.2 sCMOS camera (ANDOR Technology), interfaced with a digital imaging system (MetaFluor, Universal Imaging). Each microperfused CCD was positioned directly on the poly-D-lysine to immobilize the segment for the duration of the experiment. Following a 1-hour equilibration, CCDs were loaded with 20 μM of the acetoxymethyl (AM) ester of fura 2 (Calbiochem, catalog 344906) added to the bath for 20 minutes. The tubule was then rinsed with perfusate for 30 minutes. Fura 2–loaded CCDs were alternately excited at 340 nm and 380 nm, and images — acquired every 3 seconds — were digitized for subsequent analysis. After stable baseline 340 nm/380 nm fura 2 FIRs were obtained at a slow flow rate, the luminal flow rate was increased acutely and FIRs were monitored, using our commercially available digital image analysis system (MetaFluor, Molecular Devices).

The mean FIRs, reflecting $[Ca^{2+}]_i$, for dull (identified as PCs) and bright (identified as ICs) cells were calculated, as were the changes in FIR from baseline at specified intervals of flow. We have previously reported that ICs, characterized by high levels of carbonic anhydrase activity, generally appear brighter under epifluorescence illumination than do PCs secondary to their selective accumulation of functional fluorescent dyes delivered as AM esters, such as fura 2-AM (36, 69).

Metabolic balance studies and assessment of flow-induced K^+ excretion. IC-BKα–KO and floxed littermates (10 to 13 weeks of age) were switched from a CK to a HK diet for 10 days prior to study. Mice were then placed in a metabolic cage for approximately 1 hour and encouraged to void. Over the following 6 hours, urine was collected while mice fasted. On a subsequent experimental day, after a similar 1-hour voiding period, mice were administered 10% vol/wt sterile 0.9% saline via i.p. injection, and urine was collected in metabolic cages over the next 6 hours.

Mice were sacrificed 1 day later under 2%–5% isoflurane anesthesia. Blood was collected via cardiac puncture using a heparinized syringe. Plasma electrolytes were measured using an i-STAT handheld analyzer (Abbott Point-of-Care Inc.). Samples that were obviously hemolyzed were discarded. Aldosterone concentrations were measured in plasma samples, diluted in assay buffer to fall within the standard curve, using an aldosterone-specific ELISA kit (Enzo Life Sciences ADI-900-173), according to the manufacturer's instructions. Urine osmolality was measured using a freezing-point depression osmometer (Precision Systems Inc.). Urine electrolytes were measured by flame photometry using an IL 943 (Instrumentation Laboratory).

In separate studies, mice were placed in metabolic cages where urine was collected on a daily (24-hour) basis, and weights and food and water consumption were assessed daily. After 4 days on a control diet, mice were placed on a HK diet for 10 days.

Quantitation of BKα immunofluorescence signal intensity in DCT. Kidneys from IC-BKα–KO mice and floxed control littermates fed a HK diet for 10 days were removed, the capsule and poles were discarded, and the core was immersed in 2.5% paraformaldehyde at 4°C overnight for fixation. Afterward, tissues were cryoprotected by immersion in 30% sucrose. Coronal cryosections were cut (20-μm thick sections) and pretreated with 10 mM sodium citrate buffer (90°C for 30 minutes) for antigen retrieval, rinsed with PBS, permeabilized with 0.3% Triton X-100 in PBS (10 minutes), and blocked with a solution containing 1% BSA, 10% normal donkey serum, and 0.1% Triton X-100 in PBS (RT for 1 hour). Sections were then incubated sequentially with: chicken IgY anti-BKα antibody directed against a C-terminal epitope (3.5 μg/mL, Aves Labs) (21) overnight at 4°C, A488–donkey IgG anti–chicken IgY (3 μg/mL; Jackson ImmunoResearch, 703-545-155) for 1 hour at room temperature, rabbit anti-SLC12A3 antibody (2 μg/mL; Abcam, ab224762) overnight at 4°C, and finally A546–donkey IgG anti–rabbit IgG (4 μg/mL, Molecular Probes, A10040) for 1 hour at room temperature. After each antibody incubation, sections were rinsed once for 10 minutes at room temperature with high salt PBS (containing 0.3M NaCl) and 3 times for 10 minutes each at room temperature with PBS (0.137M NaCl). Sections from 3 IC-BKα–KO and 3 control mice were immunostained concurrently under identical conditions. After immunolabeling, sections were mounted with Vectashield mounting medium (Vector Labs, catalog H-1200) and covered with a glass coverslip for visualization by confocal microscopy.

Digital images of confocal sections (pinhole 90.0 μm; step size 1.0 μm) were collected from the cortical regions of the kidney sections, using a 63X oil immersion plan-Apochromat objective (NA 1.4) and a laser-scanning Leica SP5 DMI microscope (Leica Microsystems). Quantification of mean fluorescence intensity (MFI) of apical + subapical BKα immunostaining was performed using the Leica Application Suite software LAS X (Version: 3.7.1.21655, Leica Microsystems). Two to 8 individually identified NCC^+ cells in the wall of each tubule were selected for analysis by outlining the apical + subapical regions corresponding to the NCC-associated fluorescence (10 μm^2 median) using the freehand tool of the software. For each outlined region, the sum of grayscale pixels/area outlined corresponding to the BKα MFI in

3 sequential confocal sections was obtained. MFI data for 41 individual DCT cells from 3 KO mice (9 tubules) were normalized to the averaged MFI value for 43 DCT cells from 3 control littermates (11 tubules). Data are reported as the median and interquartile ranges for MFI ratios.

Statistics. Each experiment was performed using at least 3 mice per group. All results are expressed as mean ± SD, unless otherwise indicated. An unpaired 2-tailed Student's *t* test was used to compare differences between floxed control and IC-BKα–KO mice, whereas a paired Student's *t* test was used to compare differences between data collected in the same animal or CCD. The Mann-Whitney *U* test was used for analyses of data lacking a normal distribution. For multiple comparisons, 1-way ANOVA was used, except for daily metabolic measurements. In this experiment, daily measurements were compared with a baseline measurement the day before initiation of the HK diet, and the effects of experimental day and genotype were examined using mixed-effects modeling (to allow for missing data), with Sidak's multiple comparisons test. Statistical significance was taken as $P < 0.05$.

Study approval. All animal breeding, housing, and protocols were approved by the IACUCs at the Icahn School of Medicine at Mount Sinai, University of Pittsburgh School of Medicine, New York Medical College, and the University of Utah — facilities accredited by the American Association for the Accreditation of Laboratory Animal Care. Animals were euthanized in accordance with the NIH *Guide for the Care and Use of Laboratory Animals* (National Academies Press, 2011).

Author contributions

LMS and TRK conceived and designed the study. RCG, ECR, DF, LJN, ALM, PW, LL, ARS, WW, SS, JC, EKJ, SH, and SMM contributed to the acquisition, analysis, and/or interpretation of data for the work. RCG performed all the assays in microperfused isolated tubules including measurements of transepithelial transport and $[Ca^{2+}]_i$. ECR performed the whole animal metabolic studies. DEK provided critical reagents (mice). All authors drafted the work or revised it critically for important intellectual content and approved the final version of the manuscript.

Acknowledgments

This work was supported by NIH grants R01DK038470 (to LMS and TRK), R01HL147818 (to TRK), R21DK089275 (to DEK and LMS), P30DK079307 (the Pittsburgh Center for Kidney Research), R01DK54983 (WHW), R01DK098145 (ARS), R01DK119252 (ARS), and K08DK110332 (ECR). SMM was supported by T32DK061296 and a grant from Relypsa. Confocal microscopy was performed in the Microscopy CoRE at the Icahn School of Medicine at Mount Sinai, supported with funding from NIH Shared Instrumentation Grant (FAIN: S10OD021838). KO mice used in the study were rederived by the Mouse Genetics and Gene Targeting CoRE at the Icahn School of Medicine at Mount Sinai, which is supported by the Tisch Cancer Institute at Mount Sinai (P30 CA196521 - Cancer Center Grant Support).

Address correspondence to: Lisa M. Satlin, Department of Pediatrics, Icahn School of Medicine at Mount Sinai, Box 1198, One Gustave L. Levy Place, New York, New York 10029-6574, USA. Phone: 212.241.6933; Email: lisa.satlin@mssm.edu.

1. Frindt G, Palmer LG. Low-conductance K channels in apical membrane of rat cortical collecting tubule. *Am J Physiol*. 1989;256(1 Pt 2):F143–F151.
2. Frindt G, Palmer LG. Apical potassium channels in the rat connecting tubule. *Am J Physiol Renal Physiol*. 2004;287(5):F1030–F1037.
3. Satlin LM, Palmer LG. Apical K+ conductance in maturing rabbit principal cell. *Am J Physiol*. 1997;272(3 Pt 2):F397–F404.
4. Wang WH, Schwab A, Giebisch G. Regulation of small-conductance K+ channel in apical membrane of rat cortical collecting tubule. *Am J Physiol*. 1990;259(3 Pt 2):F494–F502.
5. Xu JZ, Hall AE, Peterson LN, Bienkowski MJ, Eessalu TE, Hebert SC. Localization of the ROMK protein on apical membranes of rat kidney nephron segments. *Am J Physiol*. 1997;273(5):F739–F748.
6. Frindt G, Palmer LG. Ca-activated K channels in apical membrane of mammalian CCT, and their role in K secretion. *Am J Physiol*. 1987;252(3 Pt 2):F458–F467.
7. Hunter M, Lopes AG, Boulpaep EL, Giebisch GH. Single channel recordings of calcium-activated potassium channels in the apical membrane of rabbit cortical collecting tubules. *Proc Natl Acad Sci USA*. 1984;81(13):4237–4239.
8. Li D, et al. Inhibition of MAPK stimulates the Ca2+ -dependent big-conductance K channels in cortical collecting duct. *Proc Natl Acad Sci USA*. 2006;103(51):19569–19574.
9. Pácha J, Frindt G, Sackin H, Palmer LG. Apical maxi K channels in intercalated cells of CCT. *Am J Physiol*. 1991;261(4 Pt 2):F696–F705.

10. Satlin LM, Palmer LG. Apical Na+ conductance in maturing rabbit principal cell. *Am J Physiol*. 1996;270(3 Pt 2):F391–F397.
11. Taniguchi J, Imai M. Flow-dependent activation of maxi K+ channels in apical membrane of rabbit connecting tubule. *J Membr Biol*. 1998;164(1):35–45.
12. Schlatter E, Bleich M, Hirsch J, Markstahler U, Fröbe U, Greger R. Cation specificity and pharmacological properties of the Ca(2+)-dependent K+ channel of rat cortical collecting ducts. *Pflugers Arch*. 1993;422(5):481–491.
13. Woda CB, Bragin A, Kleyman TR, Satlin LM. Flow-dependent K+ secretion in the cortical collecting duct is mediated by a maxi-K channel. *Am J Physiol Renal Physiol*. 2001;280(5):F786–F793.
14. Atkinson NS, Robertson GA, Ganetzky B. A component of calcium-activated potassium channels encoded by the Drosophila slo locus. *Science*. 1991;253(5019):551–555.
15. Lu R, Alioua A, Kumar Y, Eghbali M, Stefani E, Toro L. MaxiK channel partners: physiological impact. *J Physiol (Lond)*. 2006;570(Pt 1):65–72.
16. Gonzalez-Perez V, Xia XM, Lingle CJ. Functional regulation of BK potassium channels by γ1 auxiliary subunits. *Proc Natl Acad Sci USA*. 2014;111(13):4868–4873.
17. Bailey MA, et al. Maxi-K channels contribute to urinary potassium excretion in the ROMK-deficient mouse model of Type II Bartter's syndrome and in adaptation to a high-K diet. *Kidney Int*. 2006;70(1):51–59.
18. Muto S, et al. Basolateral Na+/H+ exchange maintains potassium secretion during diminished sodium transport in the rabbit cortical collecting duct. *Kidney Int*. 2009;75(1):25–30.
19. Pluznick JL, Wei P, Carmines PK, Sansom SC. Renal fluid and electrolyte handling in BKCa-beta1-/- mice. *Am J Physiol Renal Physiol*. 2003;284(6):F1274–F1279.
20. Rieg T, et al. The role of the BK channel in potassium homeostasis and flow-induced renal potassium excretion. *Kidney Int*. 2007;72(5):566–573.
21. Woda CB, et al. Ontogeny of flow-stimulated potassium secretion in rabbit cortical collecting duct: functional and molecular aspects. *Am J Physiol Renal Physiol*. 2003;285(4):F629–F639.
22. Palmer LG, Frindt G. Regulation of apical K channels in rat cortical collecting tubule during changes in dietary K intake. *Am J Physiol*. 1999;277(5):F805–F812.
23. Najjar F, et al. Dietary K+ regulates apical membrane expression of maxi-K channels in rabbit cortical collecting duct. *Am J Physiol Renal Physiol*. 2005;289(4):F922–F932.
24. Carrisoza-Gaytán R, Wang L, Schreck C, Kleyman TR, Wang WH, Satlin LM. The mechanosensitive BKα/β1 channel localizes to cilia of principal cells in rabbit cortical collecting duct (CCD). *Am J Physiol Renal Physiol*. 2017;312(1):F143–F156.
25. Alper SL, Natale J, Gluck S, Lodish HF, Brown D. Subtypes of intercalated cells in rat kidney collecting duct defined by antibodies against erythroid band 3 and renal vacuolar H+-ATPase. *Proc Natl Acad Sci USA*. 1989;86(14):5429–5433.
26. Palmer LG, Frindt G. High-conductance K channels in intercalated cells of the rat distal nephron. *Am J Physiol Renal Physiol*. 2007;292(3):F966–F973.
27. Estilo G, et al. Effect of aldosterone on BK channel expression in mammalian cortical collecting duct. *Am J Physiol Renal Physiol*. 2008;295(3):F780–F788.
28. Grimm PR, Foutz RM, Brenner R, Sansom SC. Identification and localization of BK-beta subunits in the distal nephron of the mouse kidney. *Am J Physiol Renal Physiol*. 2007;293(1):F350–F359.
29. Grimm PR, Irsik DL, Liu L, Holtzclaw JD, Sansom SC. Role of BKbeta1 in Na+ reabsorption by cortical collecting ducts of Na+-deprived mice. *Am J Physiol Renal Physiol*. 2009;297(2):F420–F428.
30. Frindt G, Palmer LG. K+ secretion in the rat kidney: Na+ channel-dependent and -independent mechanisms. *Am J Physiol Renal Physiol*. 2009;297(2):F389–F396.
31. Webb TN, et al. Cell-specific regulation of L-WNK1 by dietary K. *Am J Physiol Renal Physiol*. 2016;310(1):F15–F26.
32. Liu Y, et al. WNK1 activates large-conductance Ca2+-activated K+ channels through modulation of ERK1/2 signaling. *J Am Soc Nephrol*. 2015;26(4):844–854.
33. Bello-Reuss E. Electrophysiological identification of cell types in cortical collecting duct monolayers. *Ren Physiol Biochem*. 1991;14(1-2):1–11.
34. Koeppen BM. Electrophysiological identification of principal and intercalated cells in the rabbit outer medullary collecting duct. *Pflugers Arch*. 1987;409(1-2):138–141.
35. Liu W, Morimoto T, Woda C, Kleyman TR, Satlin LM. Ca2+ dependence of flow-stimulated K secretion in the mammalian cortical collecting duct. *Am J Physiol Renal Physiol*. 2007;293(1):F227–F235.
36. Liu W, Xu S, Woda C, Kim P, Weinbaum S, Satlin LM. Effect of flow and stretch on the [Ca2+]i response of principal and intercalated cells in cortical collecting duct. *Am J Physiol Renal Physiol*. 2003;285(5):F998–F1012.
37. Woda CB, Leite M, Rohatgi R, Satlin LM. Effects of luminal flow and nucleotides on [Ca(2+)](i) in rabbit cortical collecting duct. *Am J Physiol Renal Physiol*. 2002;283(3):F437–F446.
38. Cornelius RJ, et al. Low Na, high K diet and the role of aldosterone in BK-mediated K excretion. *PLoS ONE*. 2015;10(1):e0115515.
39. Kim SM, et al. Salt sensitivity of blood pressure in NKCC1-deficient mice. *Am J Physiol Renal Physiol*. 2008;295(4):F1230–F1238.
40. Meneton P, Loffing J, Warnock DG. Sodium and potassium handling by the aldosterone-sensitive distal nephron: the pivotal role of the distal and connecting tubule. *Am J Physiol Renal Physiol*. 2004;287(4):F593–F601.
41. Eladari D, Chambrey R, Peti-Peterdi J. A new look at electrolyte transport in the distal tubule. *Annu Rev Physiol*. 2012;74:325–349.
42. Veiras LC, et al. Sexual Dimorphic Pattern of Renal Transporters and Electrolyte Homeostasis. *J Am Soc Nephrol*. 2017;28(12):3504–3517.
43. Yu G, Cheng M, Wang W, Zhao R, Liu Z. Involvement of WNK1-mediated potassium channels in the sexual dimorphism of blood pressure. *Biochem Biophys Res Commun*. 2017;485(2):255–260.
44. Ohno A, Ohya S, Yamamura H, Imaizumi Y. Gender difference in BK channel expression in amygdala complex of rat brain. *Biochem Biophys Res Commun*. 2009;378(4):867–871.
45. Jamali K, Naylor BR, Kelly MJ, Rønnekleiv OK. Effect of 17beta-estradiol on mRNA expression of large- conductance, voltage-dependent, and calcium-activated potassium channel alpha and beta subunits in guinea pig. *Endocrine*. 2003;20(3):227–237.
46. Zenclussen ML, Casalis PA, Jensen F, Woidacki K, Zenclussen AC. Hormonal Fluctuations during the Estrous Cycle Modulate

Heme Oxygenase-1 Expression in the Uterus. *Front Endocrinol (Lausanne)*. 2014;5:32.
47. Aleksunes LM, Yeager RL, Wen X, Cui JY, Klaassen CD. Repression of hepatobiliary transporters and differential regulation of classic and alternative bile acid pathways in mice during pregnancy. *Toxicol Sci*. 2012;130(2):257–268.
48. Ji H, et al. Sex chromosome effects unmasked in angiotensin II-induced hypertension. *Hypertension*. 2010;55(5):1275–1282.
49. Arnold AP. Mouse models for evaluating sex chromosome effects that cause sex differences in non-gonadal tissues. *J Neuroendocrinol*. 2009;21(4):377–386.
50. Gambling L, Dunford S, Wilson CA, McArdle HJ, Baines DL. Estrogen and progesterone regulate alpha, beta, and gammaE-NaC subunit mRNA levels in female rat kidney. *Kidney Int*. 2004;65(5):1774–1781.
51. Yusef YR, Thomas W, Harvey BJ. Estrogen increases ENaC activity via PKCdelta signaling in renal cortical collecting duct cells. *Physiol Rep*. 2014;2(5):e12020.
52. Brunette MG, Leclerc M. Effect of estrogen on calcium and sodium transport by the nephron luminal membranes. *J Endocrinol*. 2001;170(2):441–450.
53. Riazi S, Madala-Halagappa VK, Hu X, Ecelbarger CA. Sex and body-type interactions in the regulation of renal sodium transporter levels, urinary excretion, and activity in lean and obese Zucker rats. *Gend Med*. 2006;3(4):309–327.
54. Zheng W, Shi M, You SE, Ji H, Roesch DM. Estrogens contribute to a sex difference in plasma potassium concentration: a mechanism for regulation of adrenal angiotensin receptors. *Gend Med*. 2006;3(1):43–53.
55. Roesch DM, Tian Y, Zheng W, Shi M, Verbalis JG, Sandberg K. Estradiol attenuates angiotensin-induced aldosterone secretion in ovariectomized rats. *Endocrinology*. 2000;141(12):4629–4636.
56. West CA, et al. Renal and colonic potassium transporters in the pregnant rat. *Am J Physiol Renal Physiol*. 2018;314(2):F251–F259.
57. Gidenne T, Fortun-Lamothe L. Feeding strategy for young rabbits around weaning a review of digestive capacity and nutritional needs. *Animal Science*. 2002;75(2):169–184.
58. Miller RL, et al. The V-ATPase B1-subunit promoter drives expression of Cre recombinase in intercalated cells of the kidney. *Kidney Int*. 2009;75(4):435–439.
59. Meera P, Wallner M, Toro L. A neuronal beta subunit (KCNMB4) makes the large conductance, voltage- and Ca2+-activated K+ channel resistant to charybdotoxin and iberiotoxin. *Proc Natl Acad Sci USA*. 2000;97(10):5562–5567.
60. Nehrke K, Quinn CC, Begenisich T. Molecular identification of Ca2+-activated K+ channels in parotid acinar cells. *Am J Physiol, Cell Physiol*. 2003;284(2):C535–C546.
61. Holtzclaw JD, Grimm PR, Sansom SC. Intercalated cell BK-alpha/beta4 channels modulate sodium and potassium handling during potassium adaptation. *J Am Soc Nephrol*. 2010;21(4):634–645.
62. Roy A, Al-bataineh MM, Pastor-Soler NM. Collecting duct intercalated cell function and regulation. *Clin J Am Soc Nephrol*. 2015;10(2):305–324.
63. Breton S, Brown D. Novel Proinflammatory Function of Renal Intercalated Cells. *Ann Nutr Metab*. 2018;72 Suppl 2:11–16.
64. Gueutin V, et al. Renal β-intercalated cells maintain body fluid and electrolyte balance. *J Clin Invest*. 2013;123(10):4219–4231.
65. Sausbier M, et al. Cerebellar ataxia and Purkinje cell dysfunction caused by Ca2+-activated K+ channel deficiency. *Proc Natl Acad Sci USA*. 2004;101(25):9474–9478.
66. Yue P, Zhang C, Lin DH, Sun P, Wang WH. WNK4 inhibits Ca(2+)-activated big-conductance potassium channels (BK) via mitogen-activated protein kinase-dependent pathway. *Biochim Biophys Acta*. 2013;1833(10):2101–2110.
67. Liu W, Wei Y, Sun P, Wang WH, Kleyman TR, Satlin LM. Mechanoregulation of BK channel activity in the mammalian cortical collecting duct: role of protein kinases A and C. *Am J Physiol Renal Physiol*. 2009;297(4):F904–F915.
68. Satlin LM. Postnatal maturation of potassium transport in rabbit cortical collecting duct. *Am J Physiol*. 1994;266(1 Pt 2):F57–F65.
69. Liu W, et al. Mechanoregulation of intracellular Ca2+ concentration is attenuated in collecting duct of monocilium-impaired orpk mice. *Am J Physiol Renal Physiol*. 2005;289(5):F978–F988.